Circularly polarized device for 5G-NR applications on Industry 4.0

Paulo Casmal, Andre de Souza, Gabriel Fré, Ricardo Franco and Rafael A. Penchel

***Abstract*— This work presents a 5G eMBB (Enhanced Mobile Broadband) device with a circularly polarized radio frequency front-end operating at 3.75GHz. This function enhances the system's reliability and versatility without being affected by its orientation or position. To achieve this goal, the study presents the design of a dual-polarized antenna array that is combined with a 90° hybrid coupler. The radiating structure of the antenna is then connected to a 5G eMBB commercial module, and practical results are obtained in terms of RSSI (Received Signal Strength Indication) and throughput using the circularly polarized radio interface. These results are then compared to the equivalent linear single polarization structure.**

***Keywords*— 5G, eMBB, Performance evaluation, indoor application, circular polarization.**

I. Introduction

Since mobile communications technology reached the private market, such as private LTE networks in 2010's, several companies around the globe have been exploring its benefits for operations and management [1], [2]. In the manufacturing industry, the 5G network has gained attention as a promising and viable substitute for wired-based connections. This can be attributed to the capability to provide high-speed data transfer and ultra-low latency, as well as the potential for quick reconfiguration of factory layouts, process awareness, manufacturing execution systems (MES), and continuous monitoring through highly reliable wireless sensor networks. In this context, broader coverage on the 5G-based factory is mandatory for a complete replacement of wired-based data infrastructure to the high-capacity wireless private network [3]–[5].

The present study introduces a compact, simple, and cost-effective hardware solution to facilitate 5G coverage in indoor environments. This hardware solution is designed to meet the connectivity in SMT factory's environment and substitute wired cable networks with wireless networks that offer the same levels of reliability, availability, and retainability. The hardware was designed to operate with commercial 5G eMBB modules. It features a printable antenna array that optimizes coverage in shop floor environments by enabling circular polarization on 5G terminals. As a result, this study aids in the rapid adoption of 5G technology for Industry 4.0 use cases, as it describes a scalable and cost-effective system that can be easily attached to computers, controllers, robots, and other industrial equipment [4], [6].

Paulo Casmal (paulo.casmal@facens.br), André de Souza (andre.souza@facens.br) Ricardo Franco (ricardo.franco@fit-tecnologia.org.br) e Gabriel Fré (gabriel.fre@fit-tecnologia.org.br) são vinculados ao Flextronics Instituto de Tecnologia, que financiou este trabalho. Rafael A. Penchel (rafael.penchel@unesp.br). Por questões que envolvem a política de proteção a informação do Fit, os nomes dos fabricantes das tecnologias testadas foram preservados.

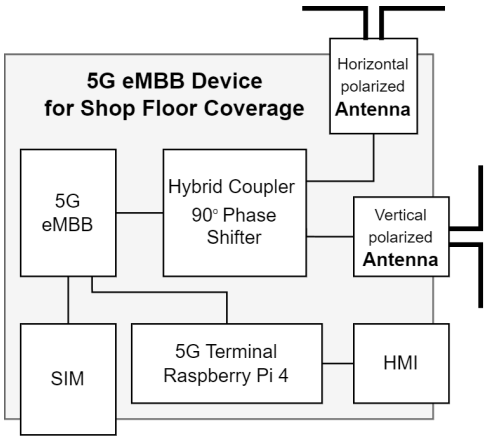

Fig. 1. Block diagram of the system including the main functional blocks to ensure the desired functionality of a 5G indoor coverage system.

In a private network context, there are costs associated with the number of operating cells in the environment, e.g. spectrum licensing, software licenses, and IT running costs, among others [7], [8]. Thereby, it is important to ensure the maximum covered area by the minimum of radio access points across the operational environment. Factory environment imposes several challenges for propagation systems, as it demands the carrier wave to penetrate and bend around obstructions [9]. Indoor communication systems typically do not require a clear line-of-sight path to operate effectively, however, obstacles of several kinds (metallic and dielectric objects) and shapes, reduce the probability of having an effective transmission [9]–[11]. In this section, it is explained the technique adopted in this work to overcome this challenge.

The block diagram presented in Fig. 1 depicts the complete system that was developed to address the aforementioned challenges. This system comprises the essential functional components necessary for enabling a 5G indoor coverage system. Specifically, the system consists of an eMBB module that is connected to a small computer that contains all the required electronics to create a 5G-ready device for general use.

This work developed a structure comprising three main functional blocks to provide a circular polarized 5G eMBB radio system. These blocks are:

1. The dual linear polarized antennas;
2. The 90° hybrid coupler; and
3. The 5G eMBB module, that provides the radio link.

By combining the three main functional blocks, a fully

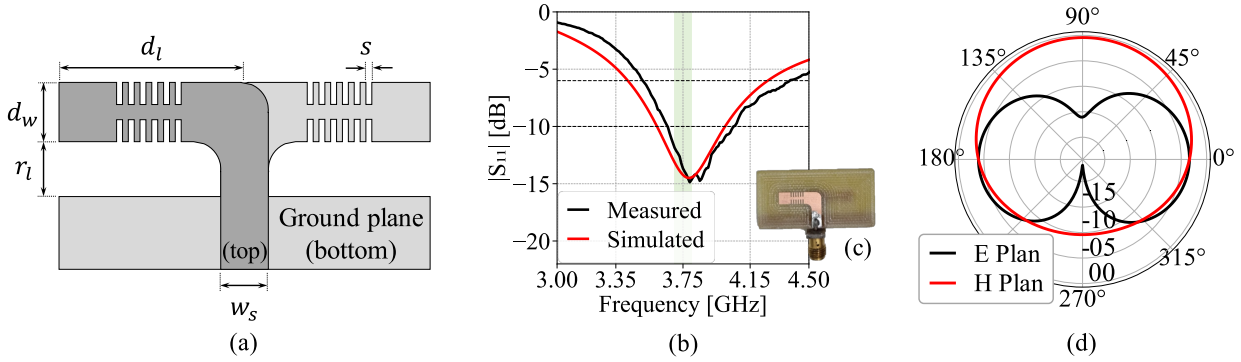

Fig. 2. Design of the half-wavelength dipole printed on FR4 PCB (printed circuit board) substrate; (a) Main dimensions and geometrical relationships; (b) Picture of the first prototype for practical evaluations; (c) Practical and simulated reflection coefficient; (d) Realized gain radiation pattern on electric and magnetic field obtained by FEM simulation.

functional 5G device capable of operation regardless of position or orientation can be achieved. This feature enhances the network range in indoor environments. Section II presents the antenna design, along with simulated and measured validations for operations at the center frequency $f_0 = 3.75$GHz. The development of the hybrid coupler is presented in Section III. Section IV provides results to demonstrate the performance improvement of using the circular polarized 5G eMBB radio system compared to a single-polarizing 5G device. The presented results aim to validate the functionality of the system and demonstrate its usefulness in applications that demand operation regardless of position or orientation. Finally, Section V offers overall conclusions and outlines further work.

II. Antennas Design

The geometry of the printed modified half-wavelength antenna dipole is depicted in Fig. 2a, the reflection coefficients of the simulated and measured final model are shown in Fig. 2b, while the simulated radiation pattern of the E and H planes are in Fig. 2c.

The model consists of two arms, each with a length (d_L) and width (d_W), printed on opposite sides of a substrate FR4 PCB (Printed Circuit Board), a microstrip transmission line with a ground plane that acts as the other component of the printed balun. The substrate has a thickness of 1.6 mm, relative permittivity, $\varepsilon_r = 4.4$ and loss tangent, $\tan\delta = 0.02$. The effective dielectric constant is evaluated with microstrip approach, in which,

$$\varepsilon_{\text{eff}} = \frac{\varepsilon_r + 1}{2}, \tag{1}$$

That value was further tuned by parametric simulations, leading to the total length L of the dipole is given by

$$L = \frac{\lambda}{2} = 2\ d_l = 24.33\,\text{mm}. \tag{2}$$

in which,

$$\lambda = \frac{\lambda_0}{\sqrt{\varepsilon_{\text{eff}}}}, \tag{3}$$

and λ_0 is the wavelength corresponding to the operating frequency $f_0 = 3.75\,\text{GHz}$ and ε_{eff} is the effective permittivity. w_s is the width of the microstrip line that feeds the antenna.

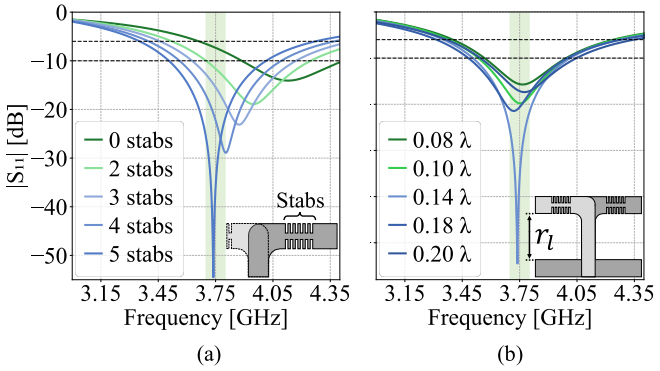

Fig. 3. Simulations results for the structure optimization. (a) Resonating frequency for different stab setups. (b) Reflection Coefficient for different relief conditions.

Nevertheless, the numerical analysis (see Fig. 3a) conducted using Ansys EM has indicated that the resonant frequency of the dipole, with the specified dimensions, falls outside the targeted range established for the project. Thus, suggesting that the effective length of the dipole is shorter than initially predicted by the design. In order to prevent enlarging the structure, small stabs were included in the dipole arms. Fig. 3a shows that five stabs were enough to ensure operations at $f_0 = 3.75\,\text{GHz}$. All the geometric parameters of the antenna are listed in Table I.

Fig. 3b presents the effect of the distance of the dipole from the ground plane r_l on the antenna reflection coefficient. One may verify that $r_l = 0.14\lambda$ yields the best performance among the considered cases. It corresponds to $6.81\,\text{mm}$. Hence, the antenna to be deployed on the 5G device proposed in this work is completely defined. The structure to provide correct phase shifting is presented in the following section.

III. The 90° hybrid coupler

The hybrid coupler is a passive component widely used in microwave engineering for the purpose of splitting or combining RF signals while maintaining a precise phase shift of 90° between the two output ports [12]–[14]. It has a variety of applications, including antenna beam-forming, beam-steering, and, specifically for the focus of this work,

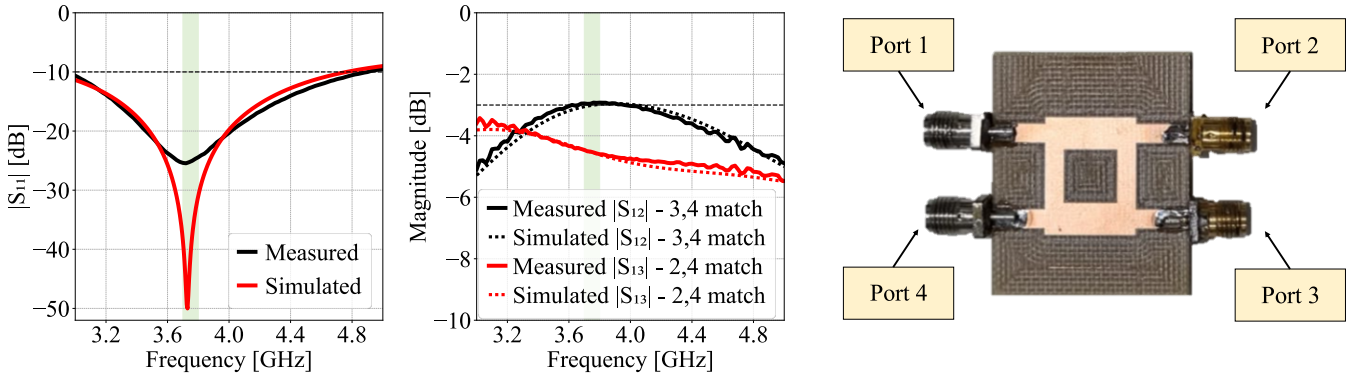

Fig. 4. The hybrid coupler applied on the design. (c) Picture of the prototype with port scheme utilized on measurements.

TABLE I
GEOMETRIC PARAMETERS IN ANTENNA DESIGN.

parameter	value [mm]	meaning
L	24.33	Total length
d_l	12.16	Dipole arm length
d_w	4.00	Dipole arm width
w_s	3.06	Feed line width
r_l	6.81 (0.14λ)	Distance from ground plane
s	0.40	Stab thickness

providing circular polarization in radio devices. This capability has been demonstrated in previous studies by Zhang et al. [15], [16].

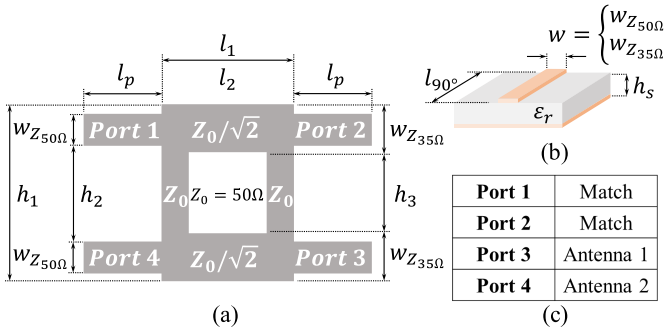

Port 1	Match
Port 2	Match
Port 3	Antenna 1
Port 4	Antenna 2

Fig. 5. The hybrid coupler applied on the design. (a) Design parameters definitions. (b) Microstrip definitions applied on hybrid design. (c) Operational conditions of the hybrid coupler.

The hybrid coupler design considers the combinations of microstrip lines in two different length and width configurations. The longitudinal elements, between Port 1 and 2 and Port 4 and 3, are modeled to present characteristic impedance $Z_0 = 50/\sqrt{2}$. The transversal element, between Port 1 and 4, and Port 2 and 3, must have $Z_0 = 50\,\Omega$. The characteristic impedance is basically evaluated from the line width, w, and the substrate height, h_s, by:

$$Z_0 = \frac{120\pi}{\sqrt{\varepsilon_{\text{eff}}}\left[(w/h_s + 1.393 + 0.667\ln(w/h_s + 1.444)\right]} \quad (4)$$

The width, w, that yields $Z_0 = 50/\sqrt{2} \equiv 35.36\,\Omega$ on the longitudinal element is $w_{Z_{35\Omega}} = 5.22\,\text{mm}$. For the transversal elements, the characteristic impedance $Z_0 = 50\,\Omega$ is obtained with $w_{Z_{50\Omega}} = 3.06\,\text{mm}$. The geometric parameters are presented in Fig. 5. The length of the elements should be set to ensure $90°$ phase shifting, between Port 2 and 3, as demonstraded in Fig. 7. This is obtained by a quarter of the wavelength, theoretically equal to $l_{90°} = 12.16\,\text{mm}$. Nevertheless, the length was tuned by FEM simulations, which indicates the optimum $l_{90°} \cong 8.60\,\text{mm}$, as demonstrated in Fig. 6. The resulting design parameters are detailed in Table II.

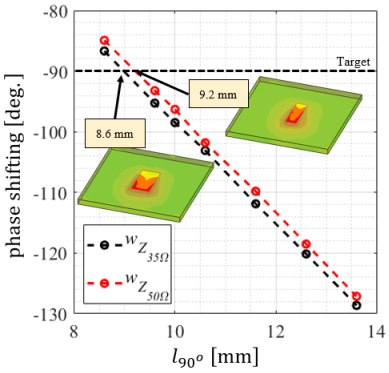

Fig. 6. Phase shifting in function of length for microstrip with $w_{Z_{50\Omega}}$ and $w_{Z_{35\Omega}}$.

TABLE II
HYBRID COUPLER DESIGN PARAMETERS.

parameter	value [mm]	meaning
l_1	14.72	Longitudinal element length
$l_2 = l_p = h_3$	8.60	Center element separation
h_1	19.04	Total height
h_2	10.76	Port separation
$w_{Z_{50\Omega}}$	3.06	Transversal element width
$w_{Z_{35\Omega}}$	5.22	Longitudinal element width
h_s	1.60	PCB substrate height

The Fig. 4 brings results from practical and simulated analysis of the hybrid coupler. One may verify in Fig. 4a an acceptable impedance matching for the input port (Port 1), below -10 dB along the n78 band, between 3.7 and 3.8 GHz. Moreover, in Fig. 4b, one may note a quite unbalanced transmission coefficient at the operating frequency $f_0 = 3.75\,\text{GHz}$,

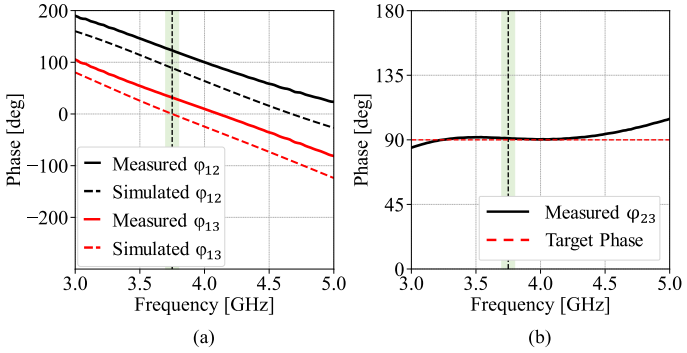

Fig. 7. Phase shifting effects on a hybrid coupler. (a) Measured and Simulated phase shifting between excitation port (Port 1) and Port 2 and 3. (b) Phase between Port 2 and 3, being the effective phase shifting on the antennas.

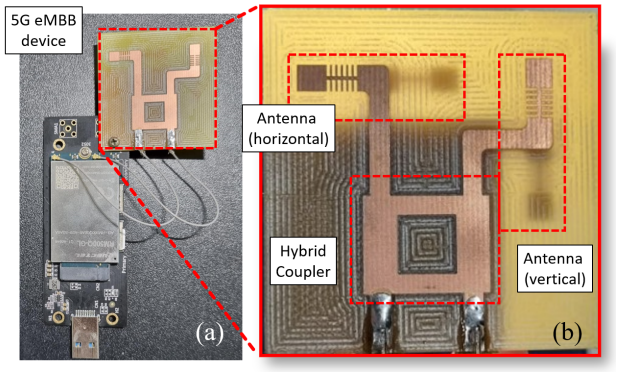

Fig. 8. The final device utilized on RSSI measurement. It consists in a eMBB module (a) with the circular polarized irradiating structure (b).

being $S_{12} = -3\,\mathrm{dB}$ and $S_{13} = -5\,\mathrm{dB}$. The best operating frequency in terms of balancing, is approximately 3.3 GHz. Besides such difference, the resulting device performance remains within limits, as seen on the next section, that brings acceptable results in terms of data transferring and signal reception.

IV. Circularly Polarized Radio System

The circular polarized irradiating system is obtained by the hybrid coupler, detailed on Section III, feeding two antennas as proposed on Section II. The antennas are displaced perpendicularly and fed with a phase difference of approximately 90 °, as demonstrated by simulations results on Fig. 4c. The final structure is presented by Fig. 8, that brings an eMBB 5G module to operate at band n78. The network interface card have four independent radios connectors, in which only Port 2 and 4 were utilized on the tests. Fig. 8b highlights the antennas displacement and the hybrid coupler attached to module ports by a pair of coaxial high-frequency cables with the same length. This device was connected to a notebook and the data about RSSI was extract by AT commands [1] sent by USB 3.0 serial interface [17]. The results in terms of throughput were taken with the network analytic tool named iPerf [18]. In both cases, it was utilized a reference device based on same module, but only capable of linear polarization [19]. Fig. 9 shows those results, in which one may verify that for both RSSI and throughput, the circular polarized setup has exhibited similar performance regardless of the board orientation. The linear polarized device demonstrated significant better performance when placed on vertical position, with more than 10 dB in terms of RSSI and a throughput around 63% superior if compared to the same module in horizontal position. The circular polarized setup, on the other hand, did not demonstrate significant difference when placed in vertical or horizontal position, with a performance slightly above the best evaluations of the linear polarized setup. Actually, simulated results has shown an axial ratio around 5 dB, even so this feature did not affect the overall system performance, as demonstrated in Fig. 9.

[1] AT commands are instructions used to control a modem

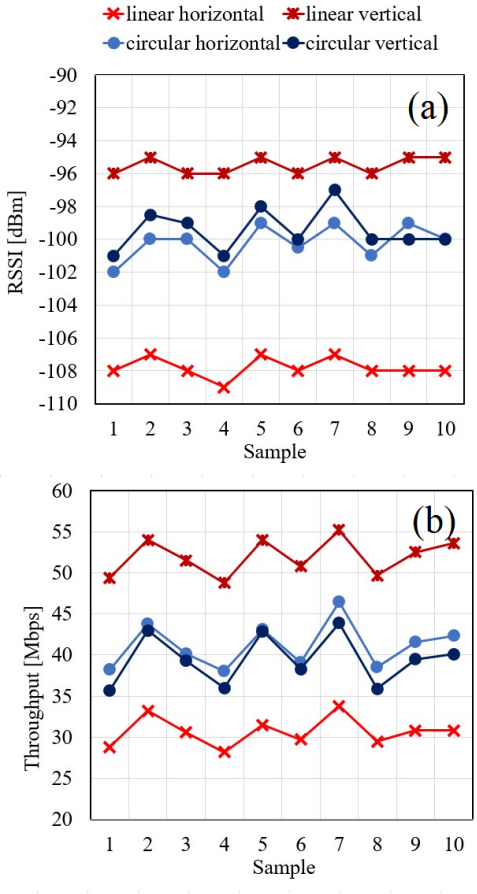

Fig. 9. Performance evaluation by application analysis of the circular polarized 5G radio system and its equivalent linear only radiation system.(a) RSSI - Received Signal Strength Indicator. (b) Throughput, um mega bits per second for both, vertical and horizontal positioning.

V. Conclusions and Further Works

The circular polarized device presented on this work has exhibited an acceptable performance in terms of data rate or throughput and RSSI if compared to this equivalent only linear polarized setup. In fact, the linear setup has achieved better performance when placed on vertical position, indicating a tied dependency to positioning and orientation. However, this work focused on industrial operations, where the position of a given device on shop floor is not always fixed or favorable for

RF transmissions. In this case, having devices less susceptible to such variations, represent a gain terms of coverage, and so on, running costs on industrial plants, as the link budgeted should result in wide areas of serving cells operations. Other techniques should be investigated in order to minimize the effects on positioning and other harmful consequences of operations in an industrial environment. Among them, one may consider beam-steering and beam-forming, two techniques that have been extensively explored on FR2 frequency range, but with few applications on sub 6 GHz.

ACKNOWLEDGEMENT

The authors want to thanks the Flextronics Institute of Technology (FIT) in Sorocaba-SP for providing material and laboratory equipment for fabricating and measuring the prototypes at the hardware development department, "Sketch-to-Scale". The authors also thank Centro Universitário Facens and Universidade Estadual de São Paulo, for supporting this research.

REFERENCES

[1] Flex, Nokia Bell Labs, "Nokia and flex to combine 5g sa private wireless and industry 4.0 expertise for advanced manufacturing solutions in brazil," *whitepaper*, 2022.

[2] Nokia Bell Labs, Qualcomm and, GE Digital, "Ge, nokia and qualcomm unveil first private lte-based trial network customized for industrial iot," *whitepaper*, 02 2017.

[3] M. Bamforth, "Private 5g vs wi-fi vs private lte," *whitepaper*, 2020.

[4] A. Aijaz, "Private 5g: The future of industrial wireless," *IEEE Industrial Electronics Magazine*, vol. 14, no. 4, pp. 136–145, 2020.

[5] G. Fré and C. D. Martino, "Lessons learned from 5g private network enabling use cases in smt industrial shop floor," *2022 IEEE Global Communications Conference (GLOBECOM)*, 2022.

[6] G. Brown and A. PRINCIPAL, "Private 5g mobile networks for industrial iot," *Heavy Reading, White Paper, Qualcomm Inc*, 2019.

[7] M. Gundall, M. Strufe, H. D. Schotten, P. Rost, C. Markwart, R. Blunk, A. Neumann, J. Grießbach, M. Aleksy, and D. Wübben, "Introduction of a 5g-enabled architecture for the realization of industry 4.0 use cases," *IEEE access*, vol. 9, pp. 25508–25521, 2021.

[8] M. Müller, D. Behnke, P.-B. Bok, M. Peuster, S. Schneider, and H. Karl, "5g as key technology for networked factories: Application of vertical-specific network services for enabling flexible smart manufacturing," in *2019 IEEE 17th International Conference on Industrial Informatics (INDIN)*, vol. 1, pp. 1495–1500, IEEE, 2019.

[9] J. Cheng, W. Chen, F. Tao, and C.-L. Lin, "Industrial iot in 5g environment towards smart manufacturing," *Journal of Industrial Information Integration*, vol. 10, pp. 10–19, 2018.

[10] Q. Dai, Y. Liu, Z. Jiang, Z. Liu, K. Zhou, and J. Wang, "Mes wireless communication networking technology based on 433mhz," in *2008 2nd International Conference on Anti-counterfeiting, Security and Identification*, pp. 110–113, 2008.

[11] B. Y. Toh, R. Cahill, and V. F. Fusco, "Understanding and measuring circular polarization," *IEEE Transactions on Education*, vol. 46, no. 3, pp. 313–318, 2003.

[12] D. M. Pozar, *Microwave engineering*. John wiley & sons, 2011.

[13] J. A. J. Ribeiro, "Engenharia de microondas: fundamentos e aplicações," *São Paulo: Érica*, 2008.

[14] B. B. Assis, L. R. Lima, A. A. Ferreira Jr, and E. C. V. Boas, "Projeto de um acoplador híbrido de 90^o para aplicações 5g em banda c," *XL Simpósio Brasileiro de Telecomunicações e Processamento de Sinais (SBrT 2022)*, 2022.

[15] P. Zhang, S. Liu, R. Chen, and X. Huang, "A reconfigurable microstrip patch antenna with frequency and circular polarization diversities," *Chinese Journal of Electronics*, vol. 25, no. 2, pp. 379–383, 2016.

[16] X. Qing and Y. Chia, "Circularly polarized circular ring slot antenna fed by stripline hybrid coupler," *Electronics Letters*, 1999.

[17] Quectel, "Rg50xx series at commands manual," tech. rep., Quectel Wireless Solution Co., Nov. 2020.

[18] A. Tirumala, "Iperf: The tcp/udp bandwidth measurement tool," *http://dast. nlanr. net/Projects/Iperf/*, 1999.

[19] G. Fré, R. Santos, R. Abud, R. Franco, and A. Luz, "Modified elliptical dipole antenna for fr1 sub-6 ghz 5g-nr," *20º Simpósio Brasileiro de Micro-ondas e Optoeletrônica*, 2022.